Ferromagnetic properties of the Zn–Mn–O system

2008 J. Phys.: Condens. Matter 20 235217

(http://iopscience.iop.org/0953-8984/20/23/235217)

J. Phys.: Condens. Matter **20** (2008) 235217 (7pp) doi:10.1088/0953-8984/20/23/235217

Ferromagnetic properties of the Zn–Mn–O system

B Babić-Stojić[1,3], D Milivojević[1], J Blanuša[1], V Spasojević[1], N Bibić[1], B Simonović[2] and D Aranđelović[2]

[1] Vinča Institute of Nuclear Sciences, PO Box 522, 11001 Belgrade, Serbia
[2] Holding Institute of General and Physical Chemistry, Studentski trg 12, 11000 Belgrade, Serbia

E-mail: babic@vin.bg.ac.yu

Received 31 January 2008, in final form 9 April 2008
Published 6 May 2008
Online at stacks.iop.org/JPhysCM/20/235217

Abstract

Polycrystalline Zn–Mn–O samples with nominal manganese concentration $x = 0.01$ and 0.10 were synthesized by a solid state reaction route using $(ZnC_2O_4{\cdot}2H_2O)_{1-x}$ and $(MnC_2O_4{\cdot}2H_2O)_x$. Thermal treatment of the samples was carried out in air at temperatures of 673, 773 and 1173 K. The samples were investigated by x-ray diffraction, thermogravimetry, differential thermal analysis, transmission electron microscopy, magnetization measurements and electron paramagnetic resonance. Room temperature ferromagnetism is observed in Zn–Mn–O samples with $x = 0.01$ thermally treated at low temperatures (673, 773 K). It seems that the ferromagnetic phase could originate from interactions between Mn^{2+} ions and acceptor defects incorporated in the ZnO crystal lattice during the thermal treatment of the samples.

1. Introduction

Semiconductor materials that exhibit ferromagnetism above room temperature (RT) have attracted considerable interest in the past few years. These materials are essential components for the development of spintronic devices. Dietl *et al* [1] predicted the existence of ferromagnetism with a Curie temperature T_C above RT in p-type ZnO and GaN doped with Mn. Ferromagnetic phase in undoped carrier and in n-type ZnO substituted with Fe, Co and Ni was also predicted [2, 3]. Since then, intensive investigation of transition-metal-doped II–VI and III–V semiconductors has been carried out. Among these materials Mn-doped ZnO is particularly interesting because of unusual magnetic properties and disagreement about both the existence and the origin of RT ferromagnetism. The first observation of RT ferromagnetism in low-temperature-processed bulk and thin-film samples of Mn-doped ZnO was reported by Sharma *et al* [4]. In this study the authors found that their results were in agreement with a model of carrier-induced ferromagnetic ordering between Mn ions in ZnO. Theoretical prediction that p-type defects in Mn-substituted ZnO can produce high-T_C ferromagnetism was confirmed experimentally by doping of Mn^{2+}:ZnO with nitrogen [5]. It was also shown that n-type defects in Mn^{2+}:ZnO introduced by Zn vapour diffusion [5] or by hydrogen annealing [6] did not stabilize long-range Mn–Mn ferromagnetic coupling. Contrary to these reports, several authors suggested that high-temperature ferromagnetism in the low-temperature-processed Mn–Zn–O samples originated from an oxygen-vacancy-stabilized metastable phase, $Mn_{2-x}Zn_xO_{3-\delta}$ [7, 8]. In addition, some recent studies show the absence of ferromagnetic ordering in bulk single-phase $Zn_{1-x}Mn_xO$ material down to 2 K [9–11]. Controversial results have also been obtained for $Zn_{1-x}Mn_xO$ thin-film samples, which extend from paramagnetic [12] to spin-glass behaviour [13] and to low-temperature ferromagnetism [14]. Various properties obtained for the Zn–Mn–O system by different methods suggest a strong dependence of the magnetic properties of this material on the synthesis conditions. In the present work we have studied structural and magnetic properties of the Zn–Mn–O samples prepared by thermal treatment in air at various temperatures in order to get better insight into the processes responsible for the observed high-temperature ferromagnetism in this material.

2. Experimental details

Polycrystalline samples of Zn–Mn–O were prepared by a solid state reaction method using zinc oxalate dihydrate

[3] Author to whom any correspondence should be addressed.

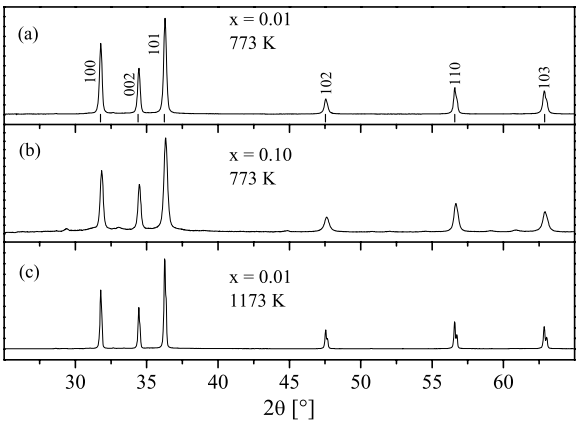

Figure 1. Full intensity x-ray diffraction patterns at 300 K for Zn–Mn–O recorded at slow scan rate: (a) $x = 0.01$ thermally treated at 773 K; (b) $x = 0.10$ thermally treated at 773 K; (c) $x = 0.01$ thermally treated at 1173 K. The vertical ticks and indices in spectrum (a) indicate the peak positions for the wurtzite crystal structure of ZnO.

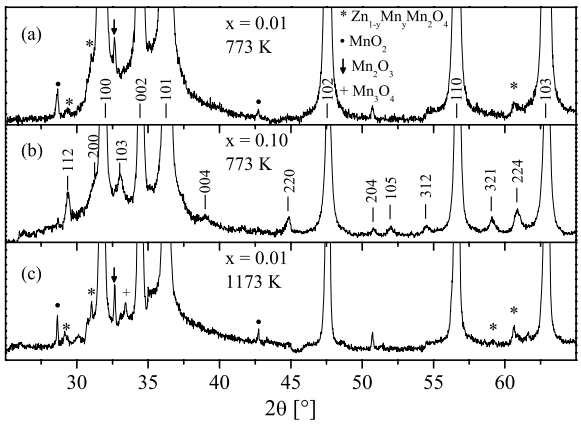

Figure 2. X-ray diffraction patterns at 300 K for Zn–Mn–O recorded at slow scan rate: (a) $x = 0.01$ thermally treated at 773 K; (b) $x = 0.10$ thermally treated at 773 K; (c) $x = 0.01$ thermally treated at 1173 K. The vertical ticks and indices in spectrum (a) indicate the peak positions for the wurtzite crystal structure of ZnO; the vertical ticks and indices in spectrum (b) indicate the peak positions of the tetragonal $ZnMn_2O_4$. Full circles, arrow, 'plus' symbol and asterisks in spectra (a) and (c) denote the secondary phases MnO_2, Mn_2O_3, Mn_3O_4 and $Zn_{1-y}Mn_yMn_2O_4$, respectively.

($ZnC_2O_4{\cdot}2H_2O$, 99.999%, Alfa Aesar) and manganese oxalate dihydrate ($MnC_2O_4{\cdot}2H_2O$, 99%, Alfa Aesar) as starting materials. Appropriate amounts of $(ZnC_2O_4{\cdot}2H_2O)_{1-x}$ and $(MnC_2O_4{\cdot}2H_2O)_x$ were mixed, pressed into pellets and calcined at 673 K for 5 h in air. The calcined samples were reground, pelletized and thermally treated at 673, 773 and 1173 K for 12 h in air to obtain Zn–Mn–O samples with a nominal manganese concentration $x = 0.01$ and 0.10.

Powder x-ray diffraction (XRD) spectra were recorded on a Philips PW 1050 diffractometer using Cu Kα radiation. XRD spectra were measured with a step size (2θ) of 0.02° at a slow scan rate of 60 s per step. Thermogravimetric analysis (TGA) and differential thermal analysis (DTA) were performed on heating up to 1273 K in a static air atmosphere at a heating rate 10° min^{-1} using a model STA-1000 (Stanton-Redcroft), which enables simultaneous recording of TGA and DTA signals. Transmission electron microscopy (TEM) measurements of Zn–Mn–O samples were carried out using a Philips EM 400 instrument with operating voltage 120 kV. The samples were prepared by placing a drop of the Zn–Mn–O water solution onto a carbon-coated copper grid. After drying, the samples were examined by TEM. The magnetization measurements were carried out on a SQUID magnetometer (MPMS XL-5, Quantum Design). Electron paramagnetic resonance (EPR) experiments were performed on a Varian E-line spectrometer operating at a nominal frequency of 9.5 GHz.

3. Results and discussion

Full intensity XRD spectra of Zn–Mn–O samples with nominal manganese concentration $x = 0.01$ and 0.10 thermally treated at 773 K and with $x = 0.01$ thermally treated at 1173 K in air are presented in figure 1. The vertical ticks and indices in spectrum (a) of figure 1 indicate the peak positions for the wurtzite crystal structure of ZnO. The XRD patterns of the same samples with recorded weakly intense peaks are shown in figure 2. It can be seen that the dominant crystal phase in the studied Zn–Mn–O samples is the wurtzite structure of ZnO (space group $P6_3mc$). The XRD data were subject to Rietveld analysis. The ZnO lattice parameters of the dominant crystal phase in the $x = 0.01$ and 0.10 samples thermally treated at 773 K are found to be very close to the crystal lattice parameters of ZnO, $a = 3.250$ Å and $c = 5.207$ Å [15]. Changes of a and c parameters with increasing temperature of thermal treatment from 673 to 1173 K are also not significant. These results are consistent with the earlier observations that the solubility of Mn in the ZnO crystal lattice is low [8, 10]. The average ZnO crystallite size determined from the width of the x-ray diffraction lines using Scherrer's formula is found to increase with increasing sintering temperature: $d \approx 30$, 60 and 100 nm for the $x = 0.01$ sample thermally treated at 673, 773 and 1173 K respectively. The XRD pattern for the $x = 0.01$ sample thermally treated at 773 K recorded at the slow scan rate reveals the existence of minor phases with low-intensity peaks, MnO_2 and a phase identified as $Zn_{1-y}Mn_yMn_2O_4$ with tetragonal symmetry (space group $I4_1/amd$). The half-maximum linewidth of the XRD peak at about 32.7° also with low intensity is found to be considerably narrower than the linewidths of the impurity phase and is attributed to Mn_2O_3 (figure 2(a)). The XRD spectrum for $x = 0.01$ thermally treated at 1173 K shows that the MnO_2 and Mn_2O_3 phases still exist at this temperature; the appearance of the Mn_3O_4 phase is also detected, whereas the impurity phase $Zn_{1-y}Mn_yMn_2O_4$ continues to grow (figure 2(c)).

In the XRD pattern of the $x = 0.10$ sample thermally treated at 773 K the impurity phase is clearly observed. We have indexed all the impurity XRD lines in this spectrum to $ZnMn_2O_4$ also with tetragonal symmetry (space group $I4_1/amd$), figure 2(b). The appearance of the impurity phase with the spinel structure $(Zn_{1-X}Mn(II)_X)[Mn(III)_2]O_4$ having cubic symmetry was detected in the Mn-doped ZnO nanoparticles prepared by a co-precipitation method after

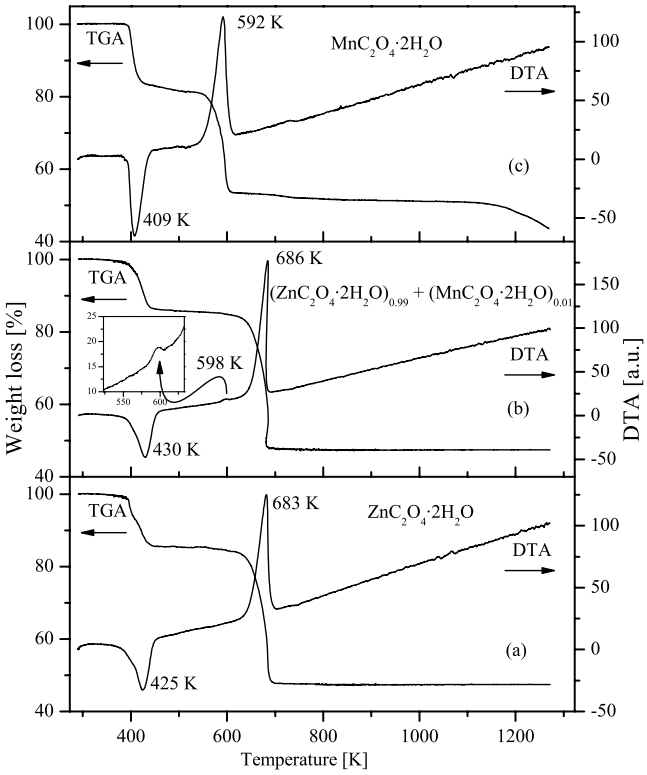

Figure 3. TGA and DTA curves for (a) $ZnC_2O_4{\cdot}2H_2O$, (b) unsintered mixture of $(ZnC_2O_4{\cdot}2H_2O)_{1-x} + (MnC_2O_4{\cdot}2H_2O)_x$ with $x = 0.01$ and (c) $MnC_2O_4{\cdot}2H_2O$.

annealing the 2% and 5% Mn-doped samples at temperatures 1075 K $< T <$ 1275 K [16]. The tetragonal phase of $ZnMn_2O_4$ was observed in the ZnMnO bulk sample with 1% Mn sintered in air at 1173 K [8]. The appearance of the $ZnMn_2O_4$ phase in our Zn–Mn–O samples at a temperature of thermal treatment as low as 773 K is probably the result of fast decomposition of the starting materials used in the synthesis.

The TGA and DTA curves for the oxalate precursors and for a sample of unsintered mixture of $(ZnC_2O_4{\cdot}2H_2O)_{1-x}$ and $(MnC_2O_4{\cdot}2H_2O)_x$ with $x = 0.01$ are presented in figure 3. Thermal decomposition of $ZnC_2O_4{\cdot}2H_2O$ occurs in two stages (figure 3(a)). The first stage is dehydration (an endothermic process with $T_{max} = 425$ K). The second stage is decomposition of anhydrous zinc oxalate (an exothermic process with $T_{max} = 683$ K). The final solid product of this decomposition found by XRD is ZnO. Thermal decomposition of the unsintered mixture of two oxalates with $x = 0.01$ occurs in three stages (figure 3(b)). The first process is dehydration of the oxalates in the unsintered $x = 0.01$ sample ($T_{max} = 430$ K). The event around $T_{max} = 686$ K involves decomposition of the zinc oxalate phase, and the process around $T_{max} = 598$ K is due to decarbonization of the manganese oxalate in this sample. The same process of decarbonization of the manganese oxalate in the starting $MnC_2O_4{\cdot}2H_2O$ material occurs around $T_{max} = 592$ K, as can be seen in figure 3(c). Taking into consideration TGA/DTA and XRD measurements it appears that the ZnO phase in the studied Zn–Mn–O samples arises as a product of decomposition of $ZnC_2O_4{\cdot}2H_2O$, whereas the MnO_2 phase detected in the $x = 0.01$ sample arises as a product of decomposition of $MnC_2O_4{\cdot}2H_2O$.

The particle size and morphology of one selected sample were characterized by transmission electron microscopy. Typical bright field TEM images of the Zn–Mn–O sample with $x = 0.01$ thermally treated at 773 K are shown in figures 4(a) and (b). TEM analysis clearly revealed the presence of two types of particles: one is elongated with faceted morphology and the other is nearly spherical in shape. This implies that two phases can be distinguished. The first is hexagonal phase, which corresponds to ZnO recorded by XRD. The size of the ZnO crystallites with faceted morphology seen by TEM lies in the range 50–100 nm, which is consistent with the result obtained from the XRD spectra. The crystallites of the second phase in the TEM images appear in the form of nearly spherical particles. Most of the crystallites of nearly spherical shape have

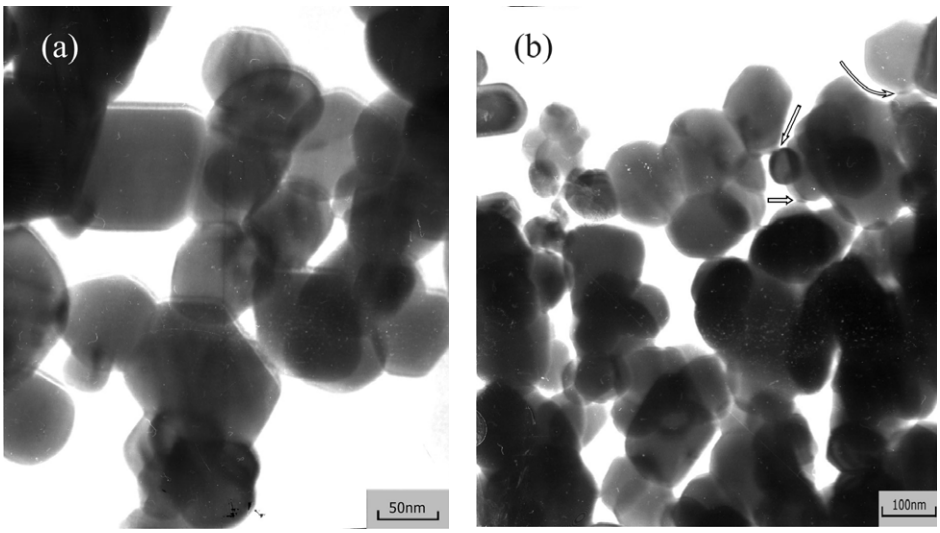

Figure 4. TEM micrographs of the $x = 0.01$ sample thermally treated at 773 K. The arrows in micrograph (b) denote the locations of coalescence of zinc oxide and manganese oxide crystallites.

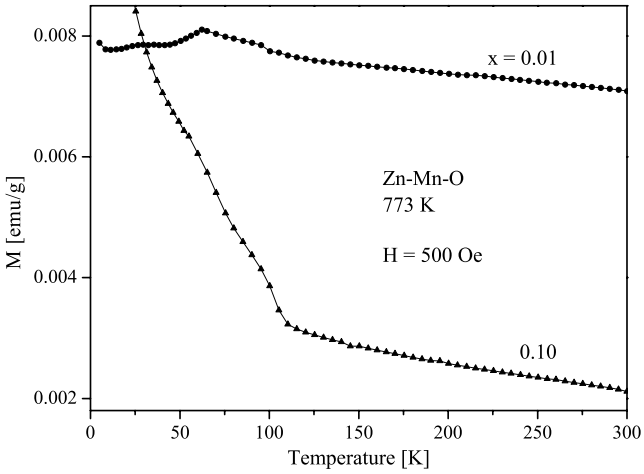

Figure 5. Temperature dependence of magnetization in the ZFC state at 500 Oe for the Zn–Mn–O samples with $x = 0.01$ and 0.10 thermally treated at 773 K.

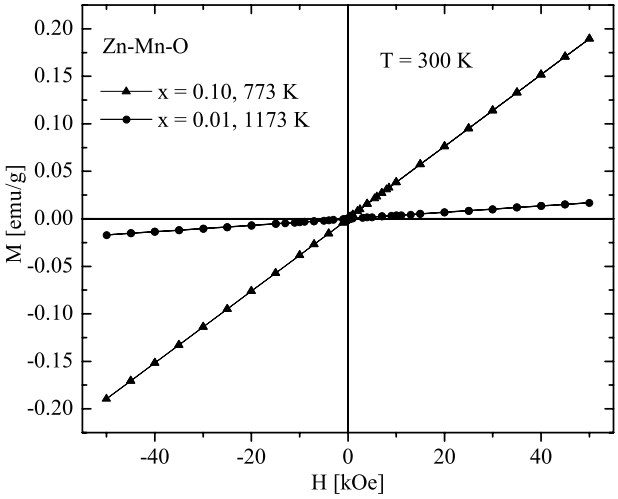

Figure 7. Field dependent magnetization at $T = 300$ K for the Zn–Mn–O samples with $x = 0.10$ thermally treated at 773 K and with $x = 0.01$ thermally treated at 1173 K.

dimensions of about 50 nm. These crystallites are attributed to the MnO_2 phase observed in the XRD spectrum of the $x = 0.01$ sample, figure 2(a). A more detailed TEM analysis of the $x = 0.01$ sample thermally treated at 773 K enabled us to clarify the coalescence of some ZnO and MnO_2 crystallites. The observed locations of coalescence of the two phases are denoted by arrows in figure 4(b).

The temperature dependence of magnetization under a magnetic field of 500 Oe for the Zn–Mn–O samples with $x = 0.01$ and 0.10 thermally treated in air at 773 K for 12 h is presented in figure 5. At higher temperatures the magnetization of the $x = 0.01$ sample is larger than that for the $x = 0.10$ sample. In addition, the sample with $x = 0.01$ shows a maximum in its $M(T)$ dependence at about 65 K in contrast to the $x = 0.10$ sample where no maximum in the $M(T)$ dependence is observed.

The magnetic field dependence of magnetization for the $x = 0.01$ sample thermally treated at 673 K is observed at $T = 250$ K (figure 6(a)) with coercive field $H_c = 80$ Oe and remanent magnetization $M_r = 0.0001$ emu g^{-1}. The $M(H)$ dependence carried out at 300 K for the $x = 0.01$ sample thermally treated at 773 K is characterized by $H_c = 800$ Oe and $M_r = 0.0050$ emu g^{-1} (figure 6(b)). Contrary to this observation, there is no RT ferromagnetism in the $x = 0.10$ sample thermally treated at 773 K. The $M(H)$ dependence for this sample is a linear function in the magnetic field range up to 50 kOe, indicating the paramagnetic origin of the magnetization at 300 K (figure 7). The absence of the RT ferromagnetism is also found in the $x = 0.01$ sample thermally treated at 1173 K. Its magnetization at 300 K can be ascribed entirely to the paramagnetic component (figure 7).

Subtracting the paramagnetic component from the total magnetization for the $x = 0.01$ samples thermally treated at 673 and 773 K, we evaluated the ferromagnetic component of the magnetization with saturation values $M_s = 0.0004$ emu g^{-1} and 0.0195 emu g^{-1} for temperatures of 673 and 773 K respectively (figure 8). It can be seen that in the

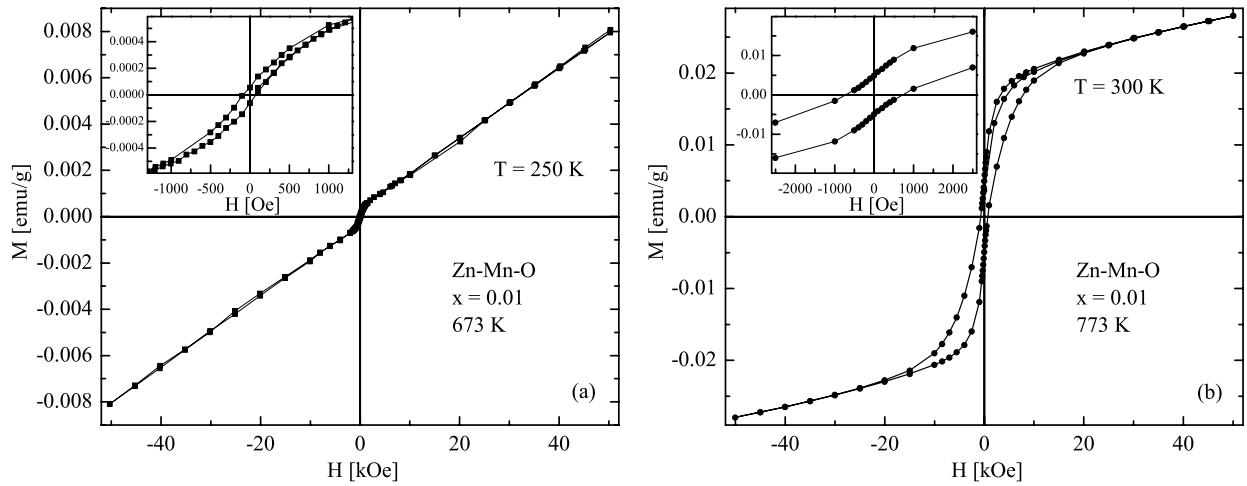

Figure 6. Field dependent magnetization curve for the Zn–Mn–O samples with $x = 0.01$ thermally treated at: (a) 673 K and (b) 773 K. The insets show details of the hysteresis loop in the low field region.

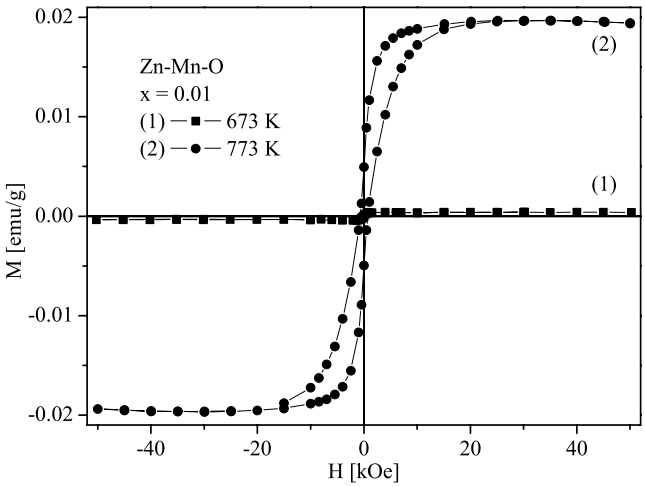

Figure 8. Ferromagnetic component of the magnetization obtained after subtracting the paramagnetic contribution for the Zn–Mn–O samples with $x = 0.01$ thermally treated at (1) 673 K and (2) 773 K measured at 250 K and 300 K, respectively.

$x = 0.01$ sample thermally treated at 773 K the coercive field is ten times larger and saturation magnetization is about 50 times larger than the corresponding values for the sample thermally treated at 673 K.

The EPR spectra of the studied Zn–Mn–O samples at 300 K are presented in figure 9. A broad resonance appears in the $x = 0.01$ sample thermally treated at 773 K on the lower field side, which disappears in the $x = 0.10$ sample thermally treated at 773 K and in the $x = 0.01$ sample thermally treated at 1173 K. The broad resonance is attributed to ferromagnetic phase in the material. The EPR spectrum in the form of fine and hyperfine lines is detected on the higher field side in all the Zn–Mn–O samples investigated (figure 9). This spectrum is analysed by the following spin Hamiltonian:

$$H = g\mu_B \mathbf{HS} + D[S_z^2 - \tfrac{1}{3}S(S+1)] + A\mathbf{SI},$$

where the first term describes the Zeeman interaction, the second term describes the axial zero-field splitting due to hexagonal symmetry of the wurtzite ZnO and the third term describes the hyperfine interaction between the electron and nuclear spins of manganese ions. For the Mn^{2+} ions $S = 5/2$, there are five fine transitions in the magnetic field **H**. Each fine transition has six hyperfine transitions due to hyperfine interaction of the Mn^{2+} ion electron spin and its nuclear spin, ^{55}Mn ($I = 5/2$). Good agreement with the experimental spectrum for the sample $x = 0.01$ thermally treated at 1173 K is obtained in the simulation using the spin-Hamiltonian parameters $A = -81$ G, $D = -252$ G and $g = 2.01$ (figure 9(d)). These values agree well with the spin-Hamiltonian parameters ($A = -81$ G, $D = -232$ G and $g = 2.0016$) reported for the Mn^{2+}-doped ZnO single crystal [17, 18]. Thus, the EPR spectrum appearing in all the Zn–Mn–O samples investigated arises from the paramagnetic moments of isolated Mn^{2+} ions substitutionally incorporated in the ZnO crystal lattice. The isolated (uncoupled) Mn^{2+} ions do not contribute to the RT ferromagnetism.

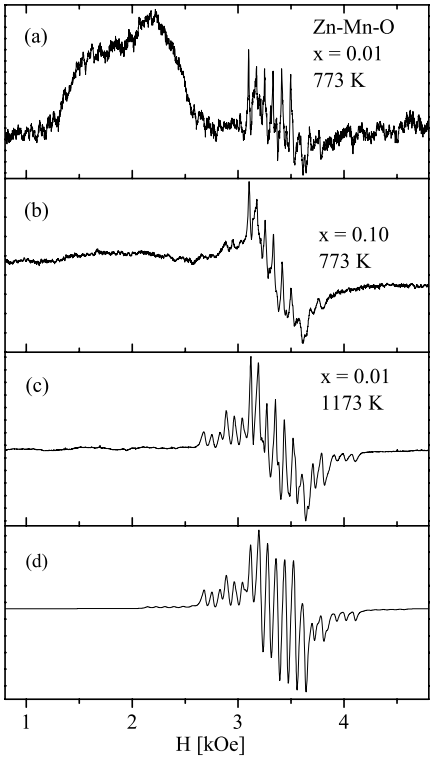

Figure 9. EPR spectra for the Zn–Mn–O samples: (a) $x = 0.01$ thermally treated at 773 K; (b) $x = 0.10$ thermally treated at 773 K; (c) $x = 0.01$ thermally treated at 1173 K; (d) simulated spectrum of Mn^{2+} ions with $S = 5/2$ and $I = 5/2$ in the ZnO crystal lattice (EPR parameters used in the simulation are $A = -81$ G, $D = -252$ G, $g = 2.01$).

Taking into account the manganese concentration in the $x = 0.01$ sample determined by an atomic absorption method, which is only a little less than that used in the synthesis, ~0.8 at.%, and the measured saturation magnetization of the ferromagnetic phase in the sample thermally treated at 773 K, the average magnetic moment per Mn ion is found to be 0.03 μ_B/Mn at 300 K. The small value of the average magnetic moment per Mn ion was reported for the bulk Mn-doped ZnO [4, 19], and also in the Mn-doped ZnO nanoparticles [16].

TEM analysis indicated that the coalescence of some zinc oxide and manganese oxide crystallites may cause the microstructural changes (figure 4(b)). It is very likely that at these locations diffusion of zinc atoms into manganese oxide occurs. Clear evidence of this process is the appearance of the impurity phase in the thermally treated Zn–Mn–O samples detected by XRD, which is identified as $Zn_{1-y}Mn_yMn_2O_4$ in the $x = 0.01$ sample and as $ZnMn_2O_4$ phase in the $x = 0.10$ sample. The reverse process of diffusion of manganese atoms into the zinc oxide crystallites also takes place. Substitutional incorporation of Mn^{2+} ions into the ZnO crystal lattice has been recorded in the EPR spectra. It has been found that the isolated Mn^{2+} ions in the ZnO crystal lattice do not contribute to the RT ferromagnetism. The RT ferromagnetism does not originate either from the $ZnMn_2O_4$ phase. The $ZnMn_2O_4$ phase with tetragonal symmetry was observed in the $x = 0.10$ sample thermally treated at 773 K, but the RT ferromagnetism was not detected in this sample. The same applies to the

$Zn_{1-y}Mn_yMn_2O_4$ phase. This impurity phase detected in the $x = 0.01$ sample progressively develops with increasing temperature of thermal treatment up to the highest temperature used in the sintering procedure, 1173 K, but the $x = 0.01$ sample thermally treated at 1173 K is fully paramagnetic at 300 K.

Besides $Zn_{1-y}Mn_yMn_2O_4$, another secondary phase detected in the $x = 0.01$ sample thermally treated at 773 K is MnO_2. This manganese oxide is antiferromagnetic, with a Néel temperature of about 84 K [20]. Pure MnO_2 transforms into Mn_2O_3 between 773 and 873 K. In the presence of Zn this transformation, which implies the reduction of $Mn^{4+} \rightarrow Mn^{3+}$, starts at lower temperatures [7]. Pure Mn_2O_3 is also antiferromagnetic, with a Néel temperature of between 80 and 100 K [21]. In the presence of Zn atoms in Mn_2O_3, incorporation of Zn into Mn^{3+} sites is possible (the ionic radius of Zn^{2+} is about 0.60 Å and the ionic radius of Mn^{3+} is about 0.58 Å [22]), and this process causes oxygen release for charge neutrality and formation of vacancies in the Mn_2O_3 structure. It is interesting to note that incorporation of Zn into Mn_3O_4, where Zn substitutes Mn^{2+} ions in the cation sublattice, leads to low-temperature ferrimagnetism similar to that of Mn_3O_4 but with lower Curie temperature [7]. In our $x = 0.01$ sample thermally treated at 673 K the RT ferromagnetism starts to develop, figure 6(a). At this temperature (673 K) a large part of the zinc oxalate is decomposed into ZnO. The abrupt increase of the ferromagnetic component of the magnetization in the $x = 0.01$ sample thermally treated at 773 K compared with that appearing at 673 K could be connected with the development of the Mn_2O_3 phase observed in the XRD spectrum (figure 2(a)), where the creation of oxygen vacancies due to presence of Zn atoms is expected. An oxygen-vacancy-stabilized metastable phase in the form $Mn_{2-x}Zn_xO_{3-\delta}$ has been suggested as a possible source of the high-temperature ferromagnetism in the low-temperature-processed Zn–Mn–O samples [7]. In several detailed studies the diffusion of Zn atoms into the manganese oxides was also considered to be responsible for the observed high-temperature ferromagnetism in the low-temperature-processed Zn–Mn–O bulk and some thin-film multilayer samples [23, 24].

However, in the recently published paper [25] the RT ferromagnetism in the $Zn_{1-x}Mn_xO$ thin films grown by pulsed laser deposition was observed even in those samples ($x < 0.03$) which have no secondary phases. The appearance of the Mn_2O_3 phase aggregating at grain boundaries was found for higher Mn concentration, $x = 0.05$, but this sample exhibited smaller saturation magnetization then that recorded for the thin films with lower manganese content. These results suggest that the high-temperature ferromagnetism in Zn–Mn–O need not be related to manganese oxides or other impurity phases and that this phenomenon is an intrinsic property of the Mn-doped ZnO material. It was established from our experimental data that the solubility of Mn in the low-temperature-processed bulk ZnO is low and that the manganese oxides exist even in the Zn–Mn–O sample with $x = 0.01$ Mn doping.

There is a possibility that a fraction of Mn ion magnetic moments incorporated in the ZnO crystal lattice in our $x = 0.01$ sample thermally treated at 773 K is ordered ferromagnetically at RT and that the ferromagnetically coupled moments coexist with the paramagnetic moments of isolated Mn ions (figure 9(a)). The coexistence of the ferromagnetically coupled Mn ion moments and paramagnetic moments of isolated Mn ions was found in the $Zn_{1-x}Mn_xO$ thin film sample with $x = 0.01$ [25], and in the 2 at.% Mn-doped ZnO nanocrystals with average particle size 12 nm annealed at 673 K [16]. This possibility focuses attention on the free charge carriers as mediators in the ferromagnetic ordering. Theoretical models have identified p-type ZnO doped with Mn as a ferromagnetic semiconductor with high T_C [1–3]. It is now well known that nitrogen is one of the most effective p-type doping agents in ZnO [26]. The film prepared from nitrogen-capped nanocrystals of 0.2 at.% Mn^{2+}:ZnO exhibited saturation magnetization of the ferromagnetically coupled Mn^{2+} ion moments of 0.75 μ_B/Mn at 300 K [5]. In the Mn-doped ZnO bulk sample with $x = 0.3$ at.% Mn prepared from ZnO and MnO_2 precursors by a sintering procedure at 773 K in air, the ferromagnetic ordering of uniformly distributed Mn^{2+} ion moments was observed with saturation magnetization of 0.16 μ_B/Mn [4]. It should be noted that the bulk Zn–Mn–O sample with 1% Mn sintered at 773 K in vacuum atmosphere exhibited weaker ferromagnetic properties at RT than the sample with 1% Mn sintered at 773 K in air [8]. Contrary to this observation, thermal treatment of the bulk $Zn_{1-x}Mn_xO$ sample with $x = 0.02$ at 873 K in an argon atmosphere resulted in considerably stronger ferromagnetic properties at 300 K than those for the sample sintered at the same temperature in air [19]. In a recent study of electrical properties of nitrogen-doped ZnO thin films it was found that the introduction of Ar in the growth ambient enhances the hole concentration and improves the N-doped ZnO conductivity [26]. For our Zn–Mn–O sample with $x = 0.01$ prepared by the solid state sintering route, which was not intentionally doped with any kind of impurity, and with final thermal treatment at 773 K in air, the saturation magnetization of the ferromagnetic phase is estimated to be 0.03 μ_B/Mn at 300 K. The very small value of the average magnetic moment per Mn ion in our ferromagnetic sample is partly the consequence of the small fraction of Mn ions which participates in the ferromagnetic ordering. The common property of almost all the Zn–Mn–O samples prepared either in the bulk form by solid state reaction method [4, 7, 8, 22, 24], or in the form of a thin film [4], or in the form of nanocrystalline particles [16], is that the RT ferromagnetism appears in the low-temperature-processed samples (673–873 K), and disappears if the samples are exposed to the high-temperature treatment (above 1073 K). The magnetic properties of the Zn–Mn–O samples observed in our study, as well as those reported by other authors, indicate that these properties are extremely sensitive to the sample preparation conditions, where the type and concentration of defects play a very important role.

According to theoretical study of the hole-mediated ferromagnetism in Mn^{2+}:ZnO [1], 3d electrons of Mn^{2+} are predicted to delocalize partially into the shallow acceptor states, thus providing exchange interaction and ferromagnetic coupling between the Mn ions. Taking into consideration the conditions of synthesis of the low-temperature-processed Zn–Mn–O samples in this study, it seems that the observed RT

ferromagnetism could originate from interactions between the Mn^{2+} ions and uncompensated acceptor defects incorporated in the ZnO crystal lattice during the thermal treatment of the samples.

4. Conclusion

Room-temperature ferromagnetism has been observed in Zn–Mn–O samples with $x = 0.01$ thermally treated at low temperatures (673 and 773 K). The structural and magnetic properties of the Zn–Mn–O samples show that it is a non-homogeneous material. An analysis of the experimental results of this work suggests that the observed RT ferromagnetism in the low-temperature-processed samples could arise from interactions between the Mn^{2+} ions and p-type defects incorporated in the ZnO crystal lattice during the thermal treatment of the samples.

Acknowledgments

Financial support for this study was granted by the Ministry of Science of the Republic of Serbia, project Nos 141013 and 141027.

References

[1] Dietl T, Ohno H, Matsukura F, Cibert J and Ferrand D 2000 *Science* **287** 1019–22
[2] Sato K and Katayama-Yoshida H 2000 *Japan. J. Appl. Phys.* **39** L555–8
[3] Sato K and Katayama-Yoshida H 2002 *Semicond. Sci. Technol.* **17** 367–76
[4] Sharma P, Gupta A, Rao K V, Owens F J, Sharma R, Ahuja R, Osorio Guillen J M, Johansson B and Gehring G A 2003 *Nat. Mater.* **2** 673–7
[5] Kittilstved K R, Norberg N S and Gamelin D R 2005 *Phys. Rev. Lett.* **94** 147209
[6] Manivannan A, Dutta P, Glaspell G and Seehra M S 2006 *J. Appl. Phys.* **99** 08M110
[7] Kundaliya D C *et al* 2004 *Nat. Mater.* **3** 709–14
[8] Zhang J, Skomski R and Sellmyer D J 2005 *J. Appl. Phys.* **97** 10D303
[9] Kolesnik S, Dabrowski B and Mais J 2004 *J. Appl. Phys.* **95** 2582–6
[10] Lawes G, Risbud A S, Ramirez A P and Seshadri R 2005 *Phys. Rev.* B **71** 045201
[11] Zhang H W, Shi E W, Chen Z Z, Liu X C and Xiao B 2006 *Solid State Commun.* **137** 272–4
[12] Tiwari A, Jin C, Kvit A, Kumar D, Muth J F and Narayan J 2002 *Solid State Commun.* **121** 371–4
[13] Fukumura T, Jin Z, Kawasaki M, Shono T, Hasegawa T, Koshihara S and Koinuma H 2001 *Appl. Phys. Lett.* **78** 958–60
[14] Jung S W, An S J, Yi G C, Jung C U, Lee S I and Cho S 2002 *Appl. Phys. Lett.* **80** 4561–3
[15] Pearton S J, Heo W H, Ivill M, Norton D P and Steiner T 2004 *Semicond. Sci. Technol.* **19** R59–74
[16] Jayakumar O D, Salunke H G, Kadam R M, Mohapatra M, Yaswant G and Kulshreshtha S K 2006 *Nanotechnology* **17** 1278–85
[17] Dorain P B 1958 *Phys. Rev.* **112** 1058–60
[18] Hausmann A and Huppertz H 1968 *J. Phys. Chem. Solids* **29** 1369–75
[19] Chen W, Zhao L F, Wang Y Q, Miao J H, Liu S, Xia Z C and Yuan S L 2005 *Appl. Phys. Lett.* **87** 042507
[20] Cullity B D 1972 *Introduction to Magnetic Materials* (Merlo park, CA: Addison-Wesley) p 157
[21] Regulski M, Przeniosło R, Sosnowska I, Hohlwein D and Schneider R 2004 *J. Alloys Compounds* **362** 236–40
[22] Bhatti K P, Chaudhary S, Pandya D K and Kashyap S C 2005 *Solid State Commun.* **136** 384–8
[23] Costa-Krämer J L, Briones F, Fernández J F, Caballero A C, Villegas M, Díaz M, García M A and Hernando A 2005 *Nanotechnology* **16** 214–8
[24] García M A *et al* 2005 *Phys. Rev. Lett.* **94** 217206
[25] Zhang J, Li X Z, Shi J, Lu Y F and Sellmyer D J 2007 *J. Phys.: Condens. Matter* **19** 036210
[26] Lu J, Liang Q, Zhang Y, Ye Z and Fujita S 2007 *J. Phys. D: Appl. Phys.* **40** 3177–81